

## Supporting Information for

# Hybrid nanostructures of pits-rich TiO<sub>2</sub> nanocrystals with Ru loading and N doping for enhanced solar water splitting

Haiqing Wang, <sup>a\*1</sup> Huiling Liu, <sup>b1</sup> Yanchen Ji, <sup>a</sup> Ruiqi Yang, <sup>a</sup> Zengfu Zhang, <sup>a</sup> Xun Wang <sup>c</sup> and Hong Liu <sup>a, d,\*</sup>

<sup>a</sup> Institute for Advanced Interdisciplinary Research (iAIR), and School of Chemistry and Chemical Engineering, University of Jinan, Jinan 250022, China

<sup>b</sup> Institute for New Energy Materials and Low-Carbon Technologies, School of Materials Science and Engineering, Tianjin Key Laboratory of Advanced Functional Porous Materials, Tianjin University of Technology, Tianjin 300384, China

<sup>c</sup> Key Lab of Organic Optoelectronics and Molecular Engineering, Department of Chemistry, Tsinghua University, Beijing 100084, China

<sup>d</sup> State Key Laboratory of Crystal Materials, Shandong University, Jinan 250100, PR China

<sup>1</sup>These authors contributed equally to the work.

## **Experimental Section**

**Chemicals.** Titanocene dichloride, zirconocene dichloride and dihafnium dichloride were purchased from TCI Industrial Co. Ferrocene,  $\text{TiCl}_4$  and tetrabutyl titanate were purchased from SCRC. All chemicals were used as received without further purification.

### **Synthesis of pits-rich $\text{TiO}_2$ nanocrystals (PTNs).**

In a typical synthesis, 0.10 g of titanocene dichloride was mixed with 20 mL of deionized water, 10 mL of ethanol and 5 mg of  $\text{NH}_4\text{F}$  under stirring. The mixture was transferred to a Teflon-lined stainless-steel autoclave and heated in an oven at 200 °C for 12 h. After reaction, the light-yellow product was separated by centrifugation and washed four times with ethanol and deionized water. The sample was dried at 60 °C overnight and then were calcinated at 500 °C for 2 h to prepare pits-rich  $\text{TiO}_2$  nanocrystals (PTNs).

### **Preparation of pits-rich $\text{TiO}_2$ -based photocatalyst ( $\text{RuO}_2$ -PTNs and Ru-N-PTNs).**

The  $\text{RuO}_2$  loading was prepared by freeze-drying and post-annealing procedures. Firstly, 20 mg  $\text{RuCl}_3$  and 100 mg PTNs were mixed in deionized water with ultrasonic for 30 min, then the mixture was dried with a freeze drier.[7] After that, the powder was homogeneously mixed and then the pits-rich  $\text{TiO}_2$ -based photocatalyst with  $\text{RuO}_2$  layer coating ( $\text{RuO}_2$ -PTNs) was obtained by annealing in air at 400 °C for 10 h. The nitrogen doping was conducted by calcination at 550 °C for 1 h, 2 h, and 3 h under  $\text{NH}_3$  atmosphere. Simultaneously, the  $\text{RuO}_2$  was reduced into metallic Ru and the product was named as Ru-N-PTNs.

**Characterization.** X-ray diffraction (XRD) patterns of the samples were measured on a Bruker D8 Advance X-ray diffractometer using Cu  $K\alpha$  radiation ( $\lambda=1.5418 \text{ \AA}$ ). Transmission electron microscopy (TEM) graphs were observed by using a Hitachi

H-7700 TEM operating at 100 kV. High-resolution transmission electron microscopy (HRTEM), high-angle annular dark-field scanning TEM (HAADF-STEM), as well as energy dispersive X-ray (EDX) element mapping tests were performed on a FEI Tecnai G2 F20 STwin microscope at 200 kV. N<sub>2</sub> adsorption-desorption isotherms were measured on a Micromeritics ASAP 2010 automatic adsorption instrument at 77 K. Before the measurements, calcined samples were degassed in vacuum at 200 °C for 2 h. Surface areas were calculated using the Brunauer-Emmett-Teller (BET) equation. Ultraviolet-visible spectrophotometry (UV-vis) absorption spectra were obtained by a Hitachi U-3900 Spectrophotometer. Thermogravimetric (TG) analysis was carried out at a heating rate of 10 °C/min from room temperature to 1000 °C under an air atmosphere (Mettler Toledo, TGA/SDTA 851e). Fourier-transform infrared (FT-IR) spectra were recorded on a Perkin Elmer FTIR spectrophotometer in the range of 4000-400 cm<sup>-1</sup> with a resolution of 4 cm<sup>-1</sup> using KBr pellet technique. The Raman spectra were recorded by a Horiba JY H-800 Raman spectrometer. X-ray photoelectron spectroscopy (XPS) signals were collected by a Thermo Fisher ESCALAB 250Xi spectrometer applying monochromatic Al K $\alpha$  X-ray sources (1486.6 eV) at 2.0 kV and 20 mA.

#### **Photocatalytic Activity Measurements.**

Photocatalytic hydrogen evolution experiments were evaluated by using a photocatalytic hydrogen evolution equipment (PerfectLight, Beijing Co., Ltd.). Typically, 0.1 g of catalyst was dispersed in 100 ml of mixed water (90 mL) and methanol (10 mL) solution with ultrasonication for 5 min. The reaction system was irradiated by using the simulated solar from Xe lamp with AM 1.5 filter and a uniform power intensity of 100 mW cm<sup>-2</sup> was calibrated. A homeothermic cooling circulation system was used to maintain the temperature of the reaction solution at 5 °C. The

online gas chromatography (GC) equipped with a TCD detector was used to determine the cumulative amount of hydrogen for every 1 h. Photocurrent generation was measured using a three-electrode system. The counter and the reference electrodes are Pt sheet and saturated calomel electrode (SCE), respectively. The electrolyte was Na<sub>2</sub>SO<sub>4</sub> aqueous solution (50 mL, 0.5 M, pH = 6.8). The IPCE of Ru-N-PTNs was measured at 320 nm light i.e. the maximum absorption position based on the UV-vis result. The 320 nm light was obtained with 300 W Xe arc lamp and a monochromator. The potential is fixed at 0.7 V (vs SCE). Incident photon to electron conversion efficiency (IPCE) detection is referred to the publication (Nano Lett. 2011, 11, 3026-3033) at the maximum absorption position of ~320 nm. The 320 nm light was obtained with 300 W Xe arc lamp (AM 1.5 G) coupled with a monochromator (CEAULIGHT). The potential is fixed at -0.6 V (vs SCE). 1 M NaOH aqueous solution (pH=13.6) was used as an electrolyte. The IPCE was calculated by the following equation:  $IPCE(\%) = 1240 I_p(\lambda) / P_{inc}(\lambda) \lambda * 100$ , where  $I_p(\lambda)$  is the photocurrent density (A m<sup>-2</sup>) and  $P_{inc}(\lambda)$  is the incident power density of light (W m<sup>-2</sup>) at wavelength  $\lambda$  (nm).

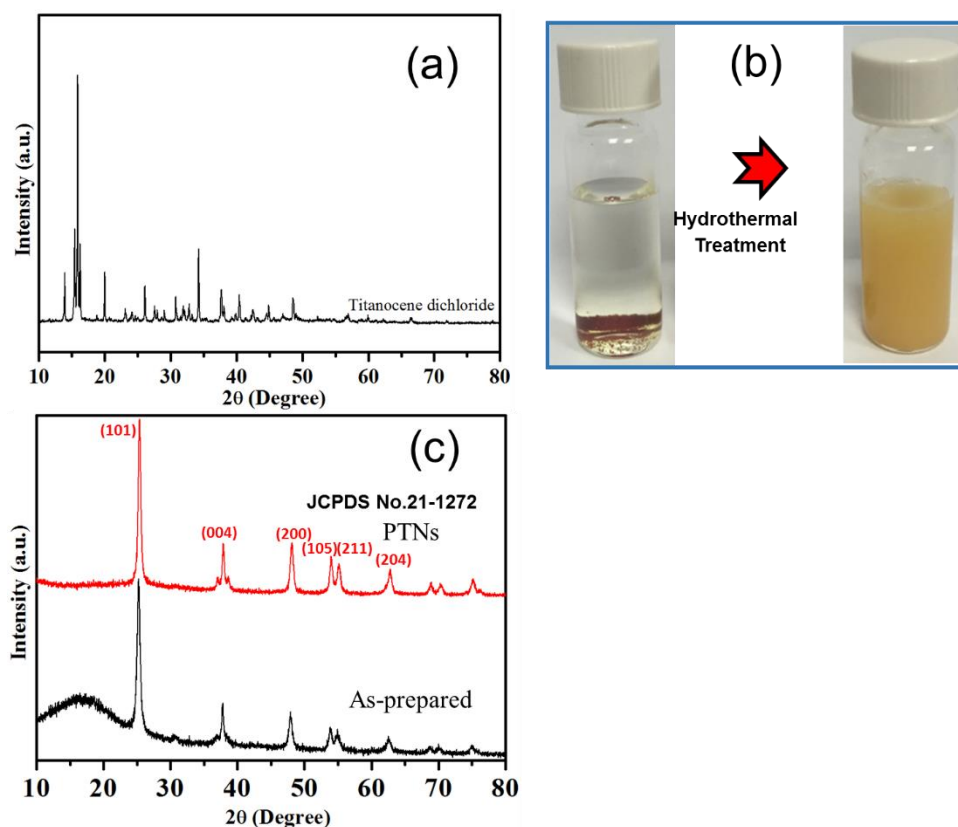


Fig. S1. XRD patterns of (a) titanocene dichloride and (c) as-prepared PTNs and PTNs, (b) digital photographs of precursor and product mixtures.

As shown in Fig. S1b, the resulting mixture turns into a yellow suspension after a hydrothermal process, despite the fact that titanocene dichloride is not dissolved into water, implying a hydrolysis procedure of the precursor at the given conditions. The grams of products can be easily prepared by a large reaction system, indicating our proposed strategy is highly reproducible for various potential applications.

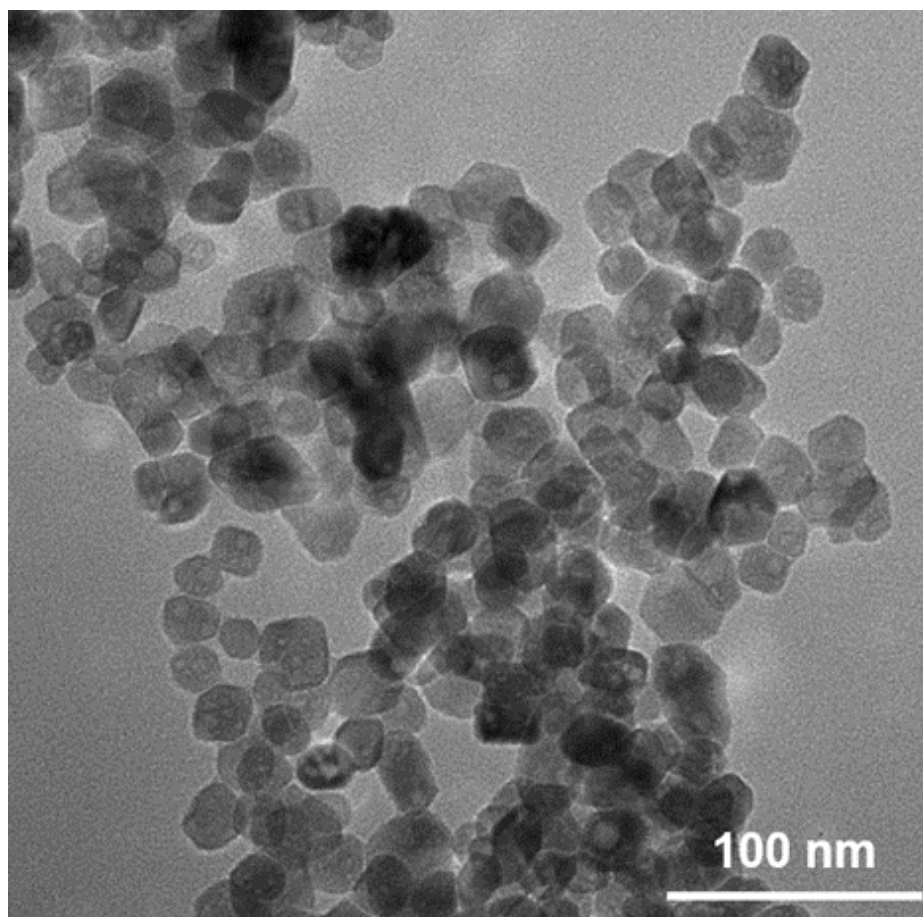


Figure S2 TEM of PTNs

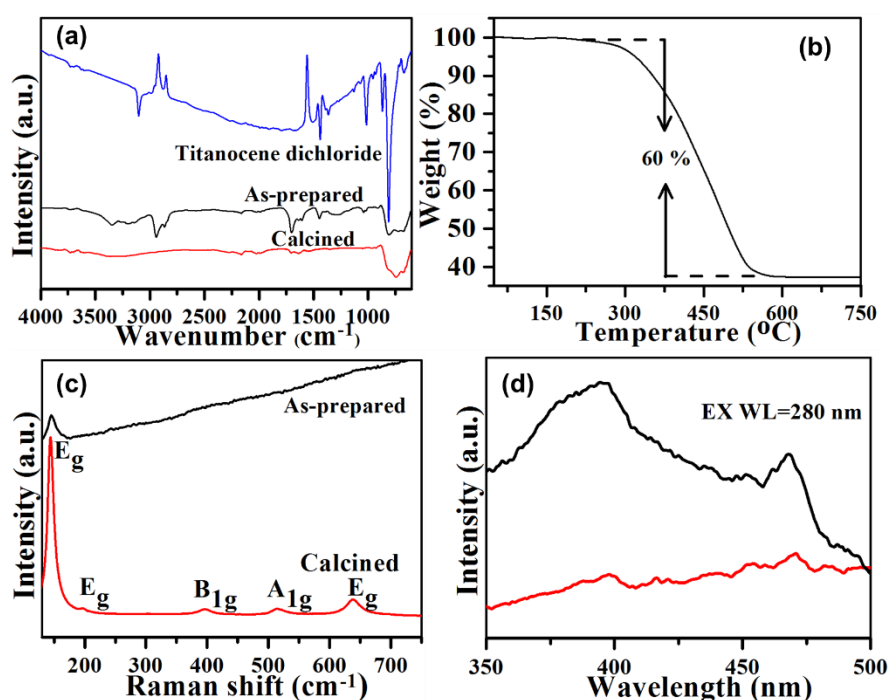


Fig. S3 TG (a), FTIR (b), Raman (c), and PL patterns of as-prepared and calcined PTNs.

The FT-IR spectra of titanocene dichloride, as-prepared and calcined PTNs were shown in Fig. S2a. The signals at ca. 700  $\text{cm}^{-1}$  of as-prepared and calcined PTNs are characteristic of the O-Ti-O lattice. The absorption bands at 3101, 1441, 1018, 814  $\text{cm}^{-1}$  in spectrum of titanocene dichloride are the characteristics of Cp ring.<sup>1</sup> The debilitated absorptions of Cp ring were still observed in as-prepared PTNs. Raman spectroscopy is a highly sensitive analytical method for crystallinity and microstructures of the materials. The Raman spectra of as-prepared and calcined PTNs are shown in Fig. S2c. The well-resolved peaks at 145 ( $E_g$ ), 198 ( $E_g$ ), 396 ( $B_{1g}$ ), 516 ( $A_{1g}$ ), and 640  $\text{cm}^{-1}$  ( $E_g$ ) in calcined sample can be attributed to the characteristic peaks of the anatase  $\text{TiO}_2$  phase. By contrast, the as-prepared sample shows only one peak at ca. 145 ( $E_g$ ) and an obvious uptrend from  $\sim 200$   $\text{cm}^{-1}$  of Raman shift related to the presence of organic impurity. As show in Fig. S2d, photoluminescence (PL) result is consistent with Raman and the lower intensity of PL for the calcined sample implies a higher efficiency of charge separation in a semiconductor. The results demonstrate the presence of pliantly of residue organics in the as-prepared PTNs. The findings imply an incomplete hydrolysis of titanocene dichloride in deionized water for the as-prepared PTNs.

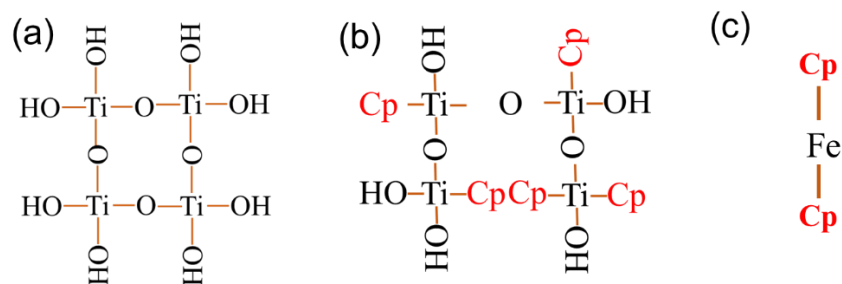


Fig. S4. The proposed nanostructures after hydrothermal process with  $\text{TiCl}_4$ ,  $\text{Cp}_2\text{TiCl}_2$ , and  $\text{Cp}_2\text{Fe}$  as precursors, respectively.

The possible hydrothermal processes with  $\text{TiCl}_4$ ,  $\text{FeCp}_2$  and  $\text{Cp}_2\text{TiCl}_2$  as precursors are proposed in Fig. S4. At the present synthesis conditions,  $\text{TiCl}_4$  can be easily hydrolyzed into  $\text{TiO}_2$  (Fig. S4a). The bonding between Fe-Cp in  $\text{FeCp}_2$  are too hard to break under this condition (Fig. S4c). While, the incomplete hydrolysis should be present in the case of  $\text{Cp}_2\text{TiCl}_2$  due to the different strength of ligands, leaving a plenty of organics in the as-prepared samples (Fig. S4b).



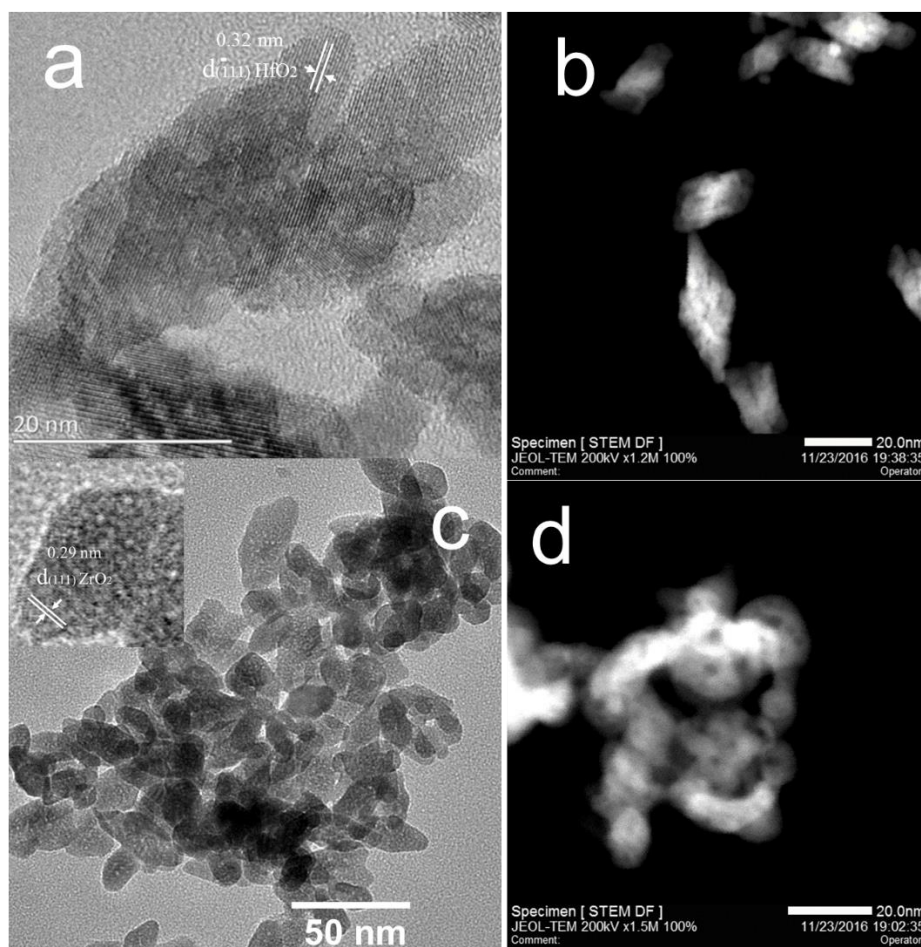


Fig. S5. HRTEM and STEM images of HfO<sub>2</sub> (a and b) and ZrO<sub>2</sub> (c and d)

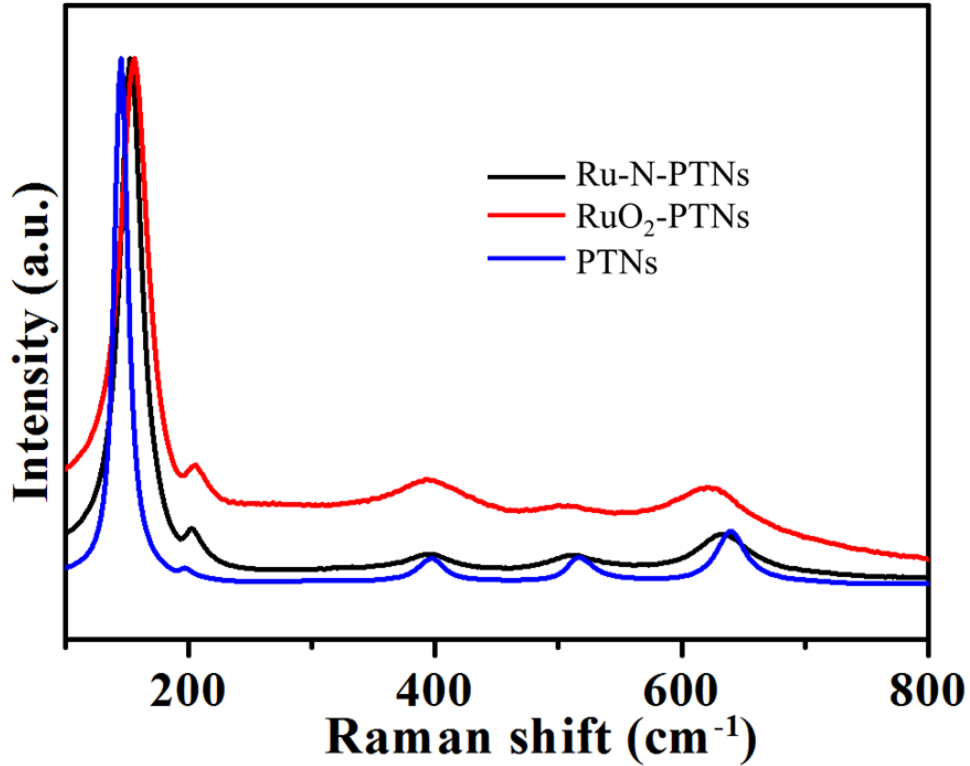


Fig. S6. Raman spectra (after normalization) of PTNs, RuO<sub>2</sub>-PTNs, and Ru-N-PTNs.

In addition, as shown in Fig. S6, the Raman spectrum of PTNs exhibits five predominant peaks at 146 cm<sup>-1</sup> (E<sub>g</sub>), 198 cm<sup>-1</sup> (E<sub>g</sub>), 399 cm<sup>-1</sup> (B<sub>1g</sub>), 516 (A<sub>1g</sub>), and 640 cm<sup>-1</sup> (E<sub>g</sub>) corresponding to anatase phase, which is in accordance with the aforementioned XRD and HRTEM results. The characteristic peaks of RuO<sub>2</sub> at 165 cm<sup>-1</sup> (B<sub>2g</sub>), 528 cm<sup>-1</sup> (E<sub>g</sub>), A<sub>1g</sub> (646 cm<sup>-1</sup>), and 716 cm<sup>-1</sup> (B<sub>2g</sub>) were not observed for RuO<sub>2</sub>-PTNs and Ru-N-PTNs.<sup>2</sup> It is worth noting that the RuO<sub>2</sub>-PTNs and Ru-N-PTNs show substantial decreasing and broadening of the Raman peaks, implying the coating of RuO<sub>2</sub> and doping of nitrogen on the substrate of PTNs.<sup>3</sup>

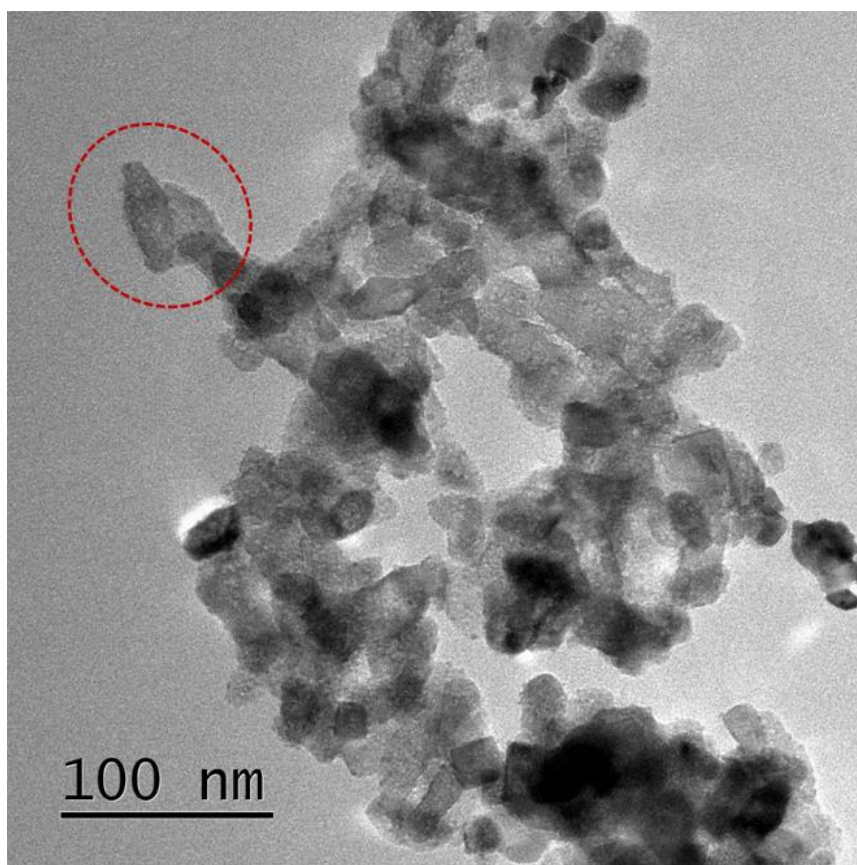


Fig. S7 The TEM image of Ru-N-PTNs.

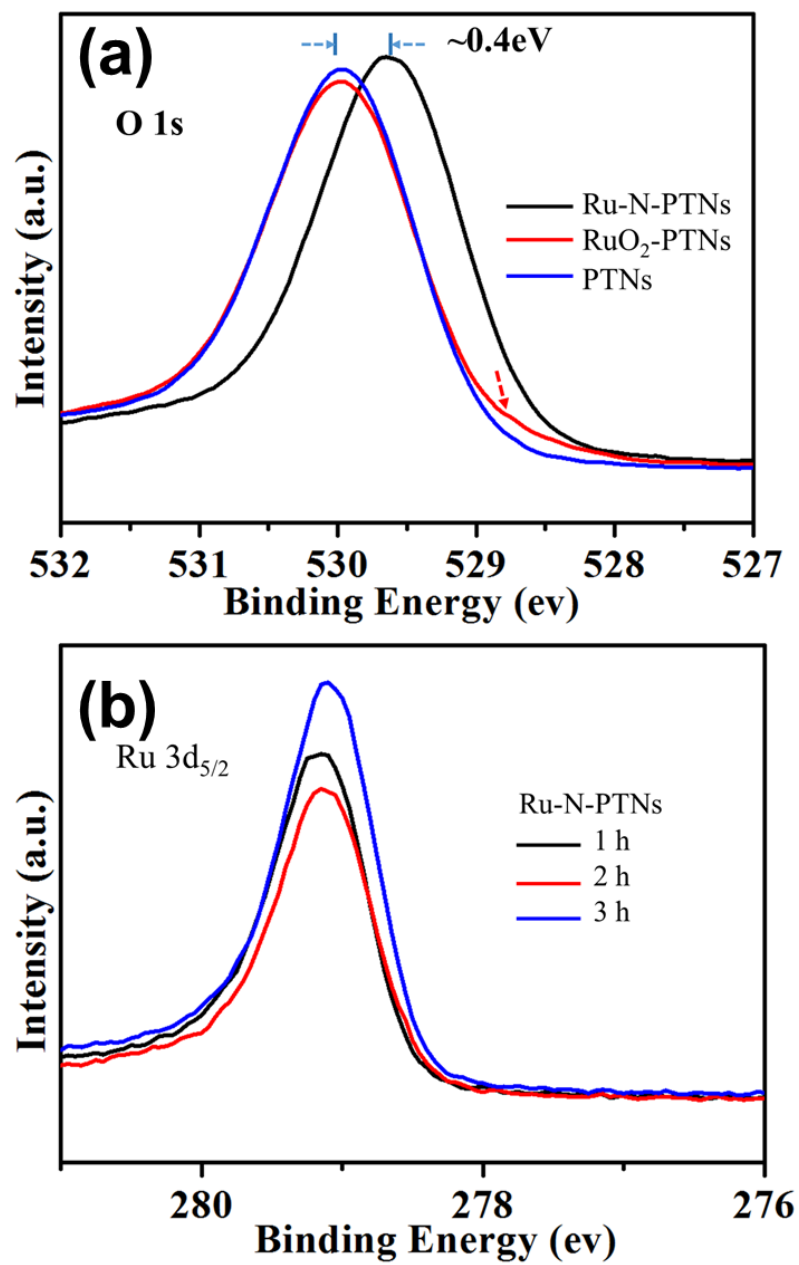


Figure S8 XPS of O 1s (a), and Ru 3d<sub>5/2</sub> (b) of samples.

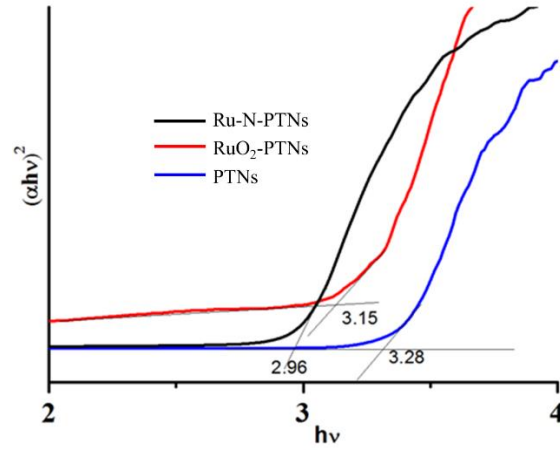


Fig. S9 the variation of  $(\alpha h\nu)^2$  with photon energy.

The energy band gap ( $E_g$ ) value of samples was obtained by absorption spectra and plotting  $(\alpha h\nu)^2$  vs photon energy ( $h\nu$ ) using the following relation:

$$(\alpha h\nu)^2 = A(h\nu - E_g) \quad (1)$$

where  $\alpha$  is the absorption coefficient,  $A$  is the constant, and  $E_g$  is the band gap of the samples, respectively. The value was calculated by extrapolating the linear portion of the curve to  $(h\nu)$  axis.

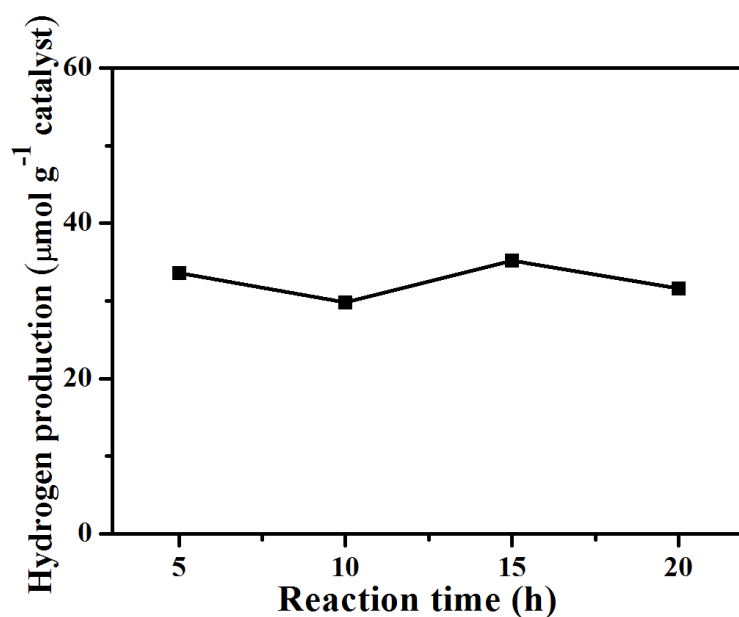


Fig. S10 The recycle stability of the Ru-N-PTNs catalysts

The recycle stability of the Ru-N-PTNs catalysts for solar water splitting was tested. The first cycle of Ru-N-PTNs provide a hydrogen production rate of  $33.6 \mu\text{mol}(\text{H}_2) \cdot \text{g}^{-1} \cdot \text{h}^{-1}$ . And, after 20 hour of four cycles, the hydrogen production rate is stabilized at  $31.8 \mu\text{mol}(\text{H}_2) \cdot \text{g}^{-1} \cdot \text{h}^{-1}$ , implying good recycle stability of the Ru-N-PTNs catalysts for solar water splitting.

## References

1. H. Wang, H. Lin, Y. Long, B. Ni, T. He, S. Zhang, H. Zhu and X. Wang, *Nanoscale*, 2017, **9**, 2074-2081.
2. M. T. Uddin, O. Babot, L. Thomas, C. Olivier, M. Redaelli, M. D'Arienzo, F. Morazzoni, W. Jaegermann, N. Rockstroh, H. Junge and T. Toupance, *J. Phys. Chem. C*, 2015, **119**, 7006-7015.
3. X. Yu, L. Wang, J. Zhang, W. Guo, Z. Zhao, Y. Qin, X. Mou, A. Li and H. Liu, *J. Mater. Chem. A*, 2015, **3**, 19129-19136.